J. Fluid Mech. (1987), *vol.* 177, *pp.* 187–206
Printed in Great Britain

Density currents or density wedges: boundary-layer influence and control methods

By GERHARD H. JIRKA AND MASAMITSU ARITA
DeFrees Hydraulics Laboratory, Cornell University, Ithaca, NY 14853, USA

(Received 14 October 1985 and in revised form 27 August 1986)

Density currents and density wedges are two observed manifestations of interactions between an ambient flow and a horizontal buoyant intrusion. In a density current the buoyant pressure force is primarily balanced by the local form drag of the current head which has a blunt shape and abrupt depth change. In a density wedge a distributed interfacial drag is the primary balancing force, leading to a stretched-out shape and long-distance intrusions. A perturbation analysis of the approach flow to the inclined front of a density current shows that slight momentum changes caused by viscous effects in the ambient flow determine which of these two flow types is established. In a uniform ambient channel flow, any momentum deficit relative to the inviscid case will lead to a local flattening of the front and ultimate breakdown into a density wedge. On the other hand, a momentum surplus will support a steady-state density current. Several exploratory experiments on control of the ambient boundary layer through local non-uniformities were performed with the objective of achieving stable density-current forms with limited intrusion lengths. These methods include a small step, a barrier and suction and are applied for intrusions at either the bottom or surface of an ambient water flow. In all cases, good agreement is found with the force balances predicted by Benjamin's (1968) theory and its extension by Britter & Simpson (1978) which accounts for entrainment in the wake zone of the head.

1. Introduction

A solid body placed in real fluid flow experiences a drag force that may be separated into a skin-friction component due to tangential stresses and a pressure (form) component due to normal stresses. Which drag component dominates in a particular instance depends on the body shape and its associated boundary-layer behaviour. Generally, long slender bodies are dominated by skin-friction drag, while short blunt bodies are characterized by early boundary layer separation and a wide wake zone, and are dominated by large form drag. Moreover, engineers have long learned to influence – for a given body shape – the type and magnitude of the drag through different methods of boundary-layer control: artificial roughness, vortex generators, boundary-layer suction, surface cooling are but a few examples. With any of these methods, a reasonably small local flow manipulation can have profound effects on the overall flow.

Several analogies can be drawn between the above fluid–solid interaction and the fluid–fluid interaction between a horizontal intrusion of a buoyant fluid and an oncoming flow. Two drastically different types of intrusion are observed experimentally (see figure 1): the *density current* and the *density wedge*.

In a density current (also called gravity current) the intrusion has a blunt body

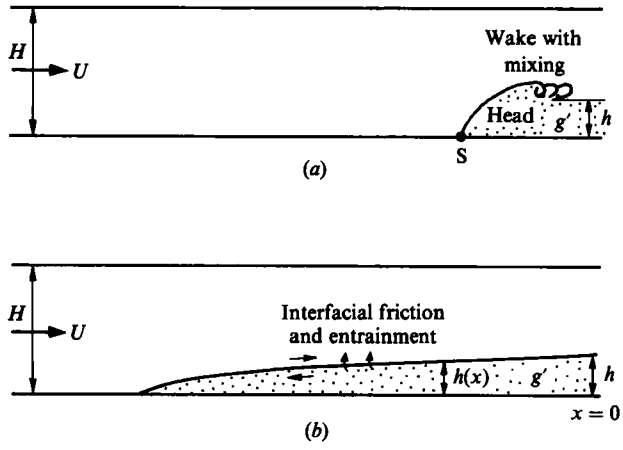

FIGURE 1. Steady-state shapes of intrusions of a dense fluid layer with buoyancy g' and initial thickness h into an ambient flow with relative velocity U (vertical average) and depth H. (*a*) Density current, (*b*) density wedge.

shape with an abrupt depth change and a distinct leading 'head'. The primary force balancing the buoyant driving force is given by a pressure drag due to the relative motion of the ambient flow around the head shape. This situation was first analysed using a bulk momentum equation by Benjamin (1968), with a later refinement by Britter & Simpson (1978) to account for the mixing in the wake zone. Usually density currents are observed in unsteady form advancing relative to a fixed reference (i.e. the ambient fluid is stagnant while the density current intrudes). However, Britter & Simpson were first to succeed in generating study density currents by using a moving belt bottom to eliminate the shear in the ambient flow.

In contrast, a density wedge exhibits an elongated body shape with a gradual depth change along the wedge length. Length-to-depth ratios of 100 in the laboratory and of 1000 in estuarine saline wedges are common. The major force balancing the buoyant intrusion force is a distributed 'skin-friction drag', i.e. the interfacial shear stress. The one-dimensional momentum equation is now employed in its differential form which, upon integration, yields a solution for the wedge shape and length. This solution was first given by Schijf & Schonfeld (1953) (see also Turner 1973) using a quadratic drag law for the interfacial shear stress. Improved solutions that would also account for the gradual mixing and entrainment over the wedge length, and thus predict the observed second-order circulation within the wedge, have not been developed to date.

Comparison with available data (see Sargent & Jirka 1982 for a recent comparative study) shows that both density currents and density wedges are adequately predicted by their respective theories. Thus we can conclude that the two intrusion types are indeed governed by rather different mechanisms, as is already suggested by their shapes. Two questions arise at this point. First, what causes a given intrusion flow to result in either of the two flow patterns? As suggested by the solid-body analogy it should be the boundary-layer behaviour along the fluid interface and – especially important in the present case – in the ambient approach flow that controls the intrusion type. Of course, a point a departure from the strict solid-body analogy is the deformability – and, to a lesser degree, the miscibility – of the interface. The suggestion that the ambient-flow boundary layer affects the type of the intrusion is

certainly not new. This has been realized by earlier investigators and, for example led Britter & Simpson to the development of their moving-belt device to generate a steady density current. What is missing, however, is a detailed linkage of the flow boundary-layer characteristics and the resulting intrusion type.

This leads to the second question: if boundary-layer control methods are successful in fluid–solid interaction, can similar methods also be used to influence the shape of the intrusion? Note, that in either case (fluid–solid interaction or intrusion flow) a control method is defined herein as a small manipulation of the boundary-layer flow that greatly affects the overall flow. It is not suggested, however, that the same types and geometrical configurations as used on solid bodies will apply for intrusion flow control. Rather, as shown below, control methods for intrusion flows work by slightly influencing the ambient approach flow ahead of the intrusion, thereby resulting in major changes of the type of the drag and – through the pressure linkage – the shape of the intrusion. Again, Britter & Simpson's moving belt clearly is such a control method but there may be other, and hopefully simpler, devices that could be systematically investigated.

Control methods are not only of fundamental interest for the study of density currents in a steady-state experimental framework, but also have important engineering applications whenever the prevention of long-distance wedge-like intrusions is desired.

In §2, a perturbation analysis of the ideal fluid flow around the forward stagnation point of a density current is used to evaluate the response of the interface to a rotational effect in the approach flow. The consequences on flow behaviour of the perturbation result are explored in §3. Then, several control methods are used experimentally to generate steady-state density currents. The results are compared to Benjamin's theory, and to Britter & Simpson's theory and experiments. Implications for engineering design are discussed in the concluding section.

2. Perturbation analysis of density-current shape

An important aspect of the density current is its forward tip which forms a stagnation point S (see figure 1*a*). Benjamin (1968) used a bulk momentum equation and a Bernoulli equation for stagnation pressure at S to derive the governing equation for the idealized density current (with inviscid approach flow and neglecting entrainment in the head wave),

$$F^2 = \frac{U^2}{g'h} = \frac{(1-n)(2-n)}{(1+n)}, \tag{1}$$

in which U is the relative speed between ambient flow and density current $g' = (\rho_2-\rho_1)g/\rho_1$ is the buoyant acceleration, $n = h/H$, where h is the intrusion thickness and H the ambient depth. Another property is the 60° angle at the stagnation point between the interface and the horizontal as first deduced by von Kármán (1940) for an inviscid ambient flow.

The following perturbation analysis demonstrates the sensitivity of the flow to small deviations from the inviscid conditions. The flow details for the corner flow near the stagnation point S are shown in figure 2. The flow is assumed to consist of the inviscid base flow (stream function ψ_0) and a superposed small perturbation flow that is rotational. In a complex polar plane (r, θ) the base flow is given by

$$\psi_0 = -Ar^m \sin[m(\theta-\pi)] \tag{2}$$

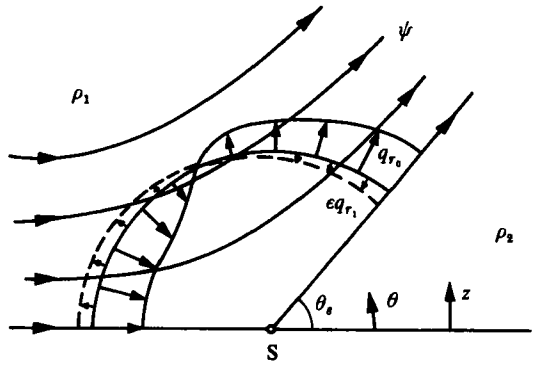

FIGURE 2. Stagnation corner flow with inviscid radial component q_{r_0} and rotational component ϵq_{r_1}.

and its radial velocity distribution $q_{0r} = (1/r)\,(\partial\psi_0/\partial\theta)$. The total radial velocity

$$\begin{aligned} q_r &= q_{r_0} + \epsilon q_{r_1} \\ &= -Ar^{m-1}m\cos[m(\theta-\pi)] + \epsilon Br^{m-1}\left[\theta-\pi+\frac{\pi}{2m}\right], \end{aligned} \tag{3}$$

in which A and B are flow constants to be chosen later and ϵ is a small dimensionless perturbation parameter that measures the magnitude of the rotational component relative to the inviscid one. The stream function ψ for the combined flow is

$$\psi = -Ar^m \sin[m(\theta-\pi)] + \epsilon Br^m\left[\tfrac{1}{2}\theta^2 - \left(\pi-\frac{\pi}{2m}\right)\theta + \left(\pi-\frac{\pi}{m}\right)\tfrac{1}{2}\pi\right], \tag{4}$$

which satisfies the no-flux conditions along $\theta = \pi$, $(\pi - \pi/m)$. In (3) an arbitrary, but simple, velocity distribution linear in θ for the rotational component q_{r_1} has been assumed.

A Bernoulli equation applies along the fluid interface with local elevation $z = r\sin\theta_s$,

$$q_r^2 = 2g'r\sin\theta_s. \tag{5}$$

Expanding the angle $\theta_s = \theta_0 + \Delta\theta$, where θ_0 is the angle under inviscid base flow and $\Delta\theta$ the perturbation of angle of order ϵ, (5) becomes

$$q_r^2 = 2g'r\sin\theta_0 + 2g'r\Delta\theta\cos\theta_0 + O(\epsilon^2). \tag{6}$$

Another expression for q_r^2 along the interface is formed from (3),

$$\begin{aligned} q_r^2 = {} & A^2m^2r^{2(m-1)}\cos^2[m(\theta_0-\pi)] \\ & -2ABm\epsilon r^{2(m-1)}\cos[m(\theta_0-\pi)]\left[\theta_0-\pi+\frac{\pi}{2m}\right] + O(\epsilon^2). \end{aligned} \tag{7}$$

Equating terms of zeroth order between (6) and (7) with consistent dependence on r gives $m = \frac{3}{2}$ and the base angle $\theta_0 = 60°$ which corresponds to von Kármán's result. The first-order solution yields the change

$$\theta_s = \theta_0 + \Delta\theta = \tfrac{1}{3}\pi - \epsilon\pi\frac{AB}{g'}. \tag{8}$$

Hence, the following dependence is obtained: any velocity deficit in the ambient flow, $\epsilon > 0$, gives $\Delta\theta < 0$, and thus flattening of the head front. Any velocity excess, $\epsilon > 0$, gives $\Delta\theta > 0$, and thus steepening of the front.

The evaluation of the constants follows so that (8) can be used for quantitative purposes. The zeroth-order terms in (6) and (7) give $A = 3^{\frac{1}{4}}(\frac{2}{3})g'^{\frac{1}{2}}$. The magnitude of the corner flow is linked to the overall flow balance of the density current so that $A = (3^{\frac{1}{4}}/F)\,(2U)/(3h^{\frac{1}{2}})$, where F is given by (1). Of course, the lengthscale of the stagnation region is given by the thickness scale h of the density current (see figure 1*a*). Thus, the above value of A together with $F = O(1)$ implies (see (6)) that the velocity scale at that distance h is equal to the ambient approach velocity U as expected. On the other hand, if the scale of the viscous influence is δ, then the base velocity at distance δ is $U(\delta/h)^{\frac{1}{2}}$. The perturbation velocity is taken as a small fraction $\epsilon U(\delta/h)^{\frac{1}{2}}$ which yields from (3) the constant $B = (3U)/(\pi h^{\frac{1}{2}})$. With these values, (8) becomes

$$\theta_s = \tfrac{1}{3}\pi - \epsilon(3^{\frac{1}{4}})\,2F. \tag{9}$$

As a numerical example, the effect of a thin boundary layer in the ambient flow may be approximated with ϵ of the order of $+0.1$. (This order of magnitude for ϵ is obtained if a turbulent boundary-layer profile is roughly matched with a linear velocity variation of equal momentum thickness with the allowance of a slip velocity at the wall). If this flow meets a shallow ($n \to 0$) density current, $F^2 = 2$ by virtue of (1), then (9) gives a flattening of the frontal interface by $\Delta\theta \approx -21°$. Two conclusions can be drawn from this. First, the shape of the head front is extremely sensitive to viscous anomalies in the flow relative to it. Secondly, the distortion effect is independent of the scale δ of the viscous influence. Even very small scales will locally distort the interface.

It is interesting to compare the above result for the distortion of the frontal angle, (9), to another perturbation approach presented recently by Rottman, Hunt & Mercer (1985). They assumed an imposed constant vorticity ζ in the corner flow and solved the governing equation for the stream function of the inviscid flow, $\nabla^2\psi = -\zeta = \text{const.}$, with appropriate interface conditions (similar to (6)). They obtained an equation for the frontal angle (in the present notation)

$$\theta_s(r) = \tfrac{1}{3}\pi + 3^{-\frac{1}{4}}\zeta r^{\frac{1}{2}}/(g')^{\frac{1}{2}}, \tag{10}$$

which is valid for small r. For $\zeta < 0$ (equivalent to $\epsilon > 0$ in the present case) this indicates flattening of the frontal face ($r > 0$), while steepening is predicted for $\zeta > 0$ (equivalent to $\epsilon < 0$). These results are qualitatively similar to the present predictions as discussed above.

Fundamentally different, however, is the behaviour right at the stagnation point, $r \to 0$. There (10) gives a fixed angle, $\theta_s(0) = \frac{1}{3}\pi$, irrespective of the ambient shear, while (9) predicts a complete distortion of the front angle, even at the smallest scale. This difference seems to be caused by the assumed vorticity distributions. While Rottman *et al.*, have assumed $\zeta = \text{const.}$, the assumed rotational velocity distribution in the present case implies a vorticity

$$\zeta = -\epsilon B r^{m-2}\left\{m^2\left[\tfrac{1}{2}\theta^2 - \left(\pi - \frac{\pi}{2m}\right)\theta + \left(\pi - \frac{\pi}{m}\right)\tfrac{1}{2}\pi\right] + 1\right\}. \tag{11}$$

Equation 11 shows maximum vorticity at the flow boundaries, $\theta = \pi, (\pi - \pi/m)$, minimum values in the flow interior, $\theta = \pi - \pi/2m$, and a singularity at $r = 0$ for the base flow case $m = \frac{3}{2} < 2$. These properties appear entirely realistic for a viscous corner flow. In particular, the singularity at the stagnation point is an inherent feature of Falkner–Skan type boundary-layer flows (e.g. Batchelor 1967) whenever $\theta_s < \frac{1}{2}$ (or $m < 2$) so that a diffuse thickening of the boundary layer starts at the stagnation point. Even though the approach flow in the present case is somewhat

different from the irrotational approach flow of the Falkner–Skan solutions it is nevertheless reasonable to expect a gradual boundary-layer growth in the accelerating flow along the density interface and hence a high localized vorticity at the leading edge of the interface, viz. the stagnation point. An exact solution of the viscous corner flow along a density front is needed. The two preliminary estimates for the front behaviour, (9) versus (10), are discussed further below in the light of experimental evidence.

3. Consequences for density intrusion

The foregoing theoretical results can be used to explain under which circumstances a particular density intrusion will occur in the form of a density current and under which in the form of a density wedge.

Any momentum deficit relative to the inviscid case in the ambient flow approaching the stagnation point causes local flattening in the head shape. This flattening, sensitive as it is, causes in turn even more viscous influence as a boundary layer between ambient and density flow develops over the flattened portion. Thus, a positive feedback occurs and the intrusion flow rapidly evolves into a wedge in which interfacial shear takes over as the balancing force. In most practical instances the momentum deficit is caused by a no-slip condition imposed on the ambient flow. Figure 3(*a*) shows two such examples: a bottom intrusion in an ambient flow with a boundary layer and a surface intrusion with contamination effects. The steady-state bottom wedge is, of course, the well-observed end product of an intrusion in riverine and estuarine applications. In our experiments, too, any bottom density current that was set up initially in accordance with Benjamin's force balance, (1), degenerated rapidly and consistently into a bottom wedge. This was true even for cases in which the current thickness h was much larger than the scale of the viscous influence, as measured by the momentum thickness of the ambient flow, so that Benjamin's bulk analysis might have been expected to hold to a first approximation. Also, in all of these cases, the front angle θ_s at the stagnation point showed a pronounced drop below 60° in accordance with (9) and in contrast to (10).

The breakdown of surface intrusions into wedges illuminates even better the scale independence of the viscous effects. In our experiments using a high-Reynolds-number flow and a wide flume (see details below) we took great care in removing any contamination (dust, floating scum) from the recirculating water flow. We adjusted the intrusion flow according to Benjamin's force balance and, indeed, were able to observe a density current for a short period. However, as some surface contamination, which is inevitably present in the flume, accumulated in the convergence zone, a local disturbance and small wedge formed at the stagnation point usually within a minute from the start of the experiment. This small wedge pushed the contamination zone ahead of it, growing in horizontal extent until the degradation into a stable wedge was complete. Detailed flow inspection, observing injected dye and neutrally buoyant particles, indicated that this contamination effect was the primary mechanism in causing the breakdown of the density current. The actual boundary-layer growth at the interface and viscous effects of the sidewalls of the wide flume seemed to be less important.

Any momentum excess relative to the inviscid case in the ambient flow approaching the stagnation point causes a stable, albeit somewhat deformed, head shape. The first example in figure 3(*b*) is the classical case of the unsteady density current advancing at a constant speed over a solid bottom. (In an actual experiment an unsteady density

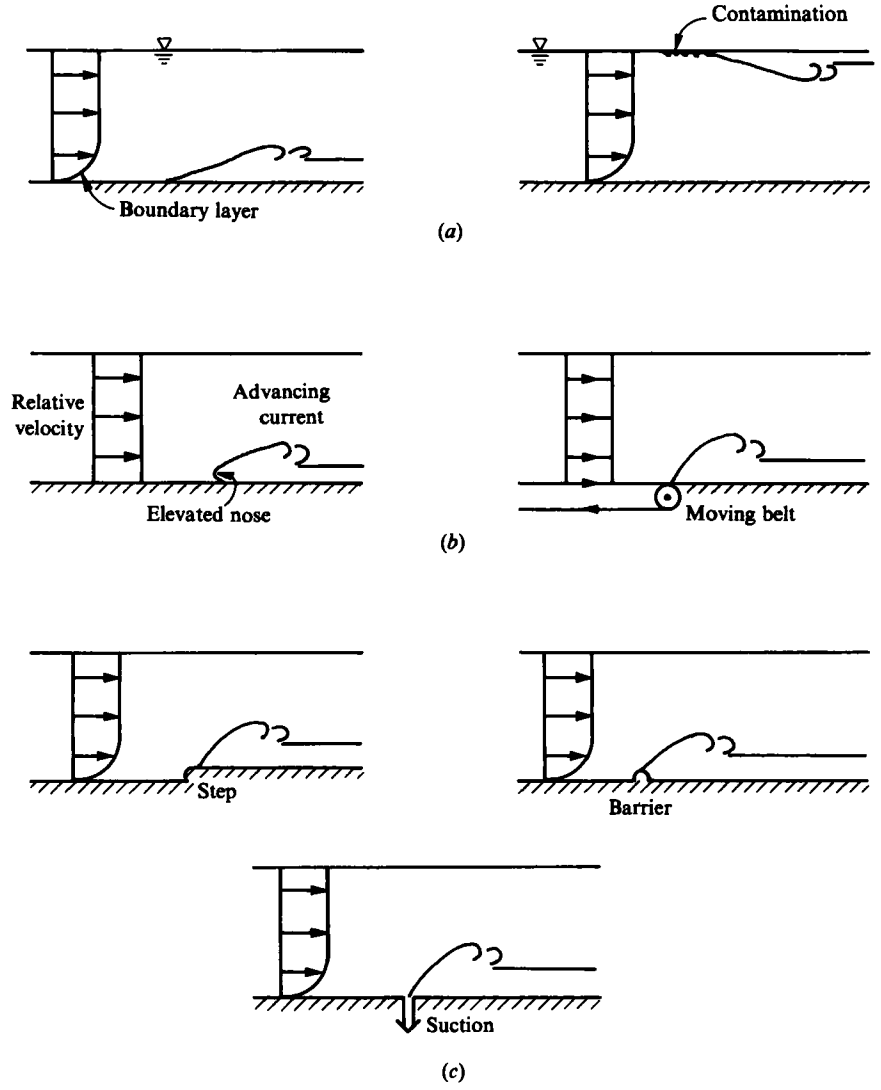

FIGURE 3. Effect of ambient flow and of boundary-layer control on the head shape of density currents. (*a*) Unstable density currents evolving into wedges, (*b*) stable density currents in a uniform channel, (*c*) stable density currents with local channel non-uniformities (control methods).

current is generated by starting at $t = 0$, and then maintaining, a constant release of buoyant fluid at a fixed position x_0. The entire flow at any time $t > 0$ is then made up of a density current as the leading element followed by a wedge-like flow with a gradual thickness increase all the way back to x_0. As time advances, a larger fraction of the buoyant force prescribed at x_0 is balanced by interfacial shear along the wedge-like flow. Consequently, both the speed of advance and the size h (see figure 1*a*) of the density current diminish over time (e.g. see Sargent & Jirka 1982). The time change is small, however, and the local flow dynamics at the density-current head can be considered as quasi-steady, so that both the steady-state fundamental force balances (e.g. (1)) and the perturbation results should hold). As the ambient flow (relative to an observer moving with the density current) approaches the head the no-slip condition at the solid bottom prevents stagnation as in the inviscid case.

Rather, the excess momentum causes such extreme steepening of the front that ambient fluid is in effect swept under the advancing density current which then exhibits the typical elevated nose. Once again, this feature is consistent with the steepening effect predicted by (9), while it does not agree with Rottman *et al.*'s (1985) prediction, (10), as $\theta(0)$ greatly exceeds $\frac{1}{3}\pi$ (see also the photographs of Simpson & Britter 1980). The ambient fluid trapped under the intrusion nose rises through convective instabilities causing the typical lobe-and-cleft structure when viewed from above (see Simpson 1982).

A momentum excess is also provided by the moving-belt device of Britter & Simpson (1978, see figure 3*b*) as the no-slip condition at the belt carries ambient-momentum fluid toward the tip of the density current. Simpson & Britter did not report any local steepening of the current shape. However, this effect can be very localized and in our experience detailed observations are very difficult. Furthermore, the downward motion of the belt may have inadvertently removed some of the boundary-layer fluid through suction, an effect similar to the suction method described below.

In a later study (Simpson & Britter 1980) the moving-belt device was used differently from the configuration sketched in figure 3(*b*). The density current was arrested directly over the moving belt, which was operated under three speed conditions: (i) a belt speed equal to the density-current speed U (this corresponds exactly to the advancing current of figure 3(*b*) as discussed above); (ii) a belt speed less than U; and (iii) a belt speed greater than U. Of course, all three cases represent a momentum excess in the ambient shear flow, but with varying magnitude. The effect is weakest for case (ii), which hence causes the least front steepening and smallest lifting of the nose, and is strongest for case (iii) as is clearly shown in Simpson & Britter's photographs (also given in Rottman *et al.* 1985).

4. Experiments on control methods for density intrusions

The discussion in the preceeding section applied to a uniform ambient-flow geometry. If local non-uniformities of sufficient magnitude are introduced into the ambient-flow channel, then additional possibilities arise for arresting intrusions in form of stable density currents. These local non-uniformities are referred to as control methods. Examples are sketched in figure 3(*c*). The general role of any of these control methods is to counteract or eliminate the velocity deficit in the ambient approach flow. This is achieved by forcing a localized high-velocity region or a flow separation, or through removal of the low-velocity fluid.

Three specific methods of influencing the boundary layer of the ambient shear flow were studied in exploratory experiments (see figure 3*c*): a step increase in elevation (first investigated by Sargent & Jirka 1982); a small barrier; and suction of the boundary layer. Similar options can be employed for density currents at the free surface.

These control methods were investigated in a recirculating stratified-flow flume (7.3 m long, 46 cm wide, 30 cm deep). The flume ends in a large stilling basin from which the ambient flow is withdrawn with a selective withdrawal device and recirculated back to the upstream end. The buoyant intrusion flow is supplied via a discharge device that is inserted at the downstream flume end. The device can be set either at the bottom or at the water surface with a variable opening height. The boundary-layer control devices were installed about 4–5 water depths upstream from the flume end.

Bottom density currents were generated through steady salt water releases, while heated water was used for surface density currents. In either case the procedure was as follows: the mean ambient velocity U and water depth H were set. Then the intrusion fluid with buoyant acceleration g' was released through the discharge device that was set to an opening height roughly corresponding to Benjamin's inviscid solution, (1). The rate of buoyant-fluid release was increased in gradual steps until a stable equilibrium density-current shape was established. At this stage the density-current tip was located at any of the boundary-layer control devices and the buoyant make-up flow was lost through mixing in the wake zone behind the head wave. The equilibrium situation was clearly distinguishable. Any further increase in supply flow (or decrease in U or increase in g') would result in an upstream advance of the density current beyond the control devices as the density-current force balance was no longer maintained. Vice versa, a decrease in the supply flow (or increase in U or decrease in g') resulted in a stretching and flattening of the density-current head with approach to a density-wedge-like appearance as a larger fraction of the intrusion force was balanced by interfacial shear.

At equilibrium, the following observations were made: the buoyant-layer thickness immediately behind the head wave was obtained from a traversing conductivity-probe record or alternatively from a shadowgraph picture using the caustic zone of maximum light intensity. The buoyant-discharge flow rate q was read from a rotameter, making sure that this flow did indeed enter the current head and did not short circuit directly into the ambient flow after release through the discharge device. These observations, together with the values of U, H and g' were then used for comparison with the appropriate theories and with Britter & Simpson's past experiments. The ambient velocity ranged between 2.5 and 7 cm/s, the buoyancy between 1.6 and 8 cm/s^2, the intrusion-layer thickness between 1 and 3 cm with an ambient water depth of about 15 cm, Thus, the ambient-flow Reynolds number UH/ν, where ν is the kinematic viscosity, was between 4000 and 13000 indicating turbulent approach flow. The layer Reynolds number Uh/ν was smaller by the factor $n = h/H$, but well above 500, the value below which Simpson (1982) reports increasing viscous influences. Further experimental details are given in Sargent & Jirka (1982).

Shadowgraphs for three different boundary-layer control devices are shown in figure 4. Figure 4(*a*) shows a step-like displacement device of 2.2 cm thickness at the bottom of an ambient approach flow of 17.6 cm so that the water depth over the device is 15.4 cm. The mean velocity profile upstream of the device is shown in figure 5. It closely resembles a $\frac{1}{7}$-power layer for which the displacement thickness is one eighth of the flow depth, $17.6/8 = 2.2$ cm. The intended role of the displacement device with approximately that thickness is then to contract the flow locally and thereby eliminate the boundary-layer momentum deficit. The step device was rounded with a 1 cm radius and no flow separation was observed. Limited velocity measurements in the absence of a density intrusion showed the essential elimination of the ambient boundary layer at the step shoulder at which a new boundary layer starts to develop. More extensive measurements approximately one-half of a water depth further downstream show a largely uniform profile with a thin boundary layer (figure 5). The stable density current that intrudes into this ambient flow up to the step shoulder (figure 4*a*) has a structure and appearance, including the formation of breaking Kelvin–Helmholtz waves, quite similar to Britter & Simpson's (1978) shadowgraph observations with their moving-belt device. Further quantitative data are discussed below.

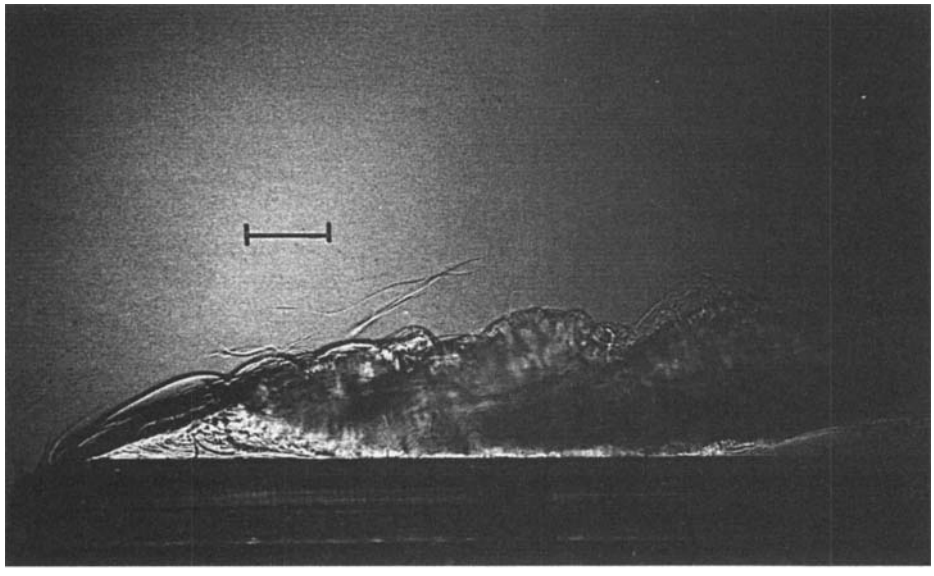

(a)

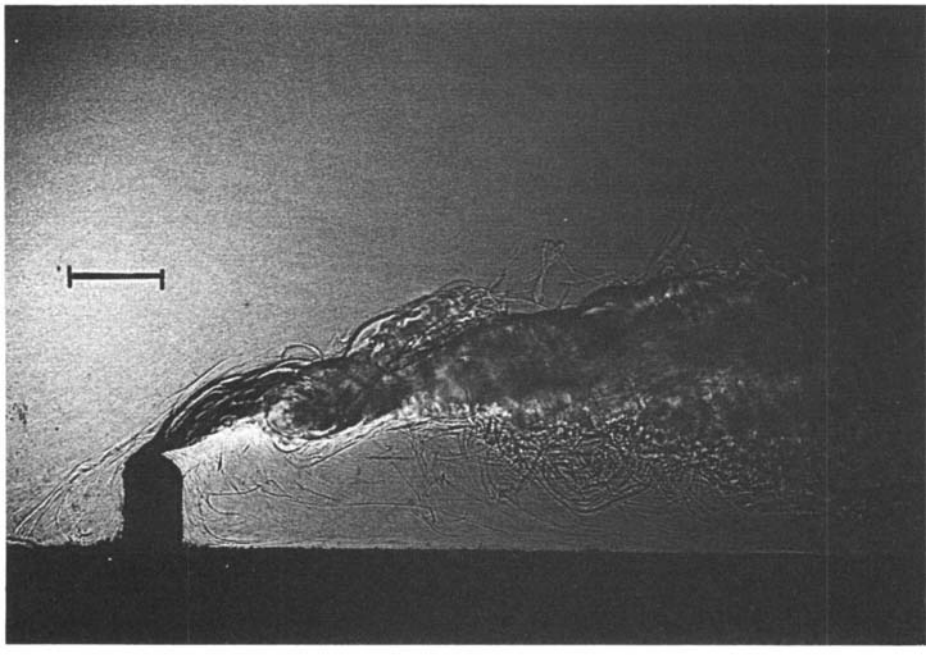

(b)

FIGURE 4(a,b). For caption see facing page.

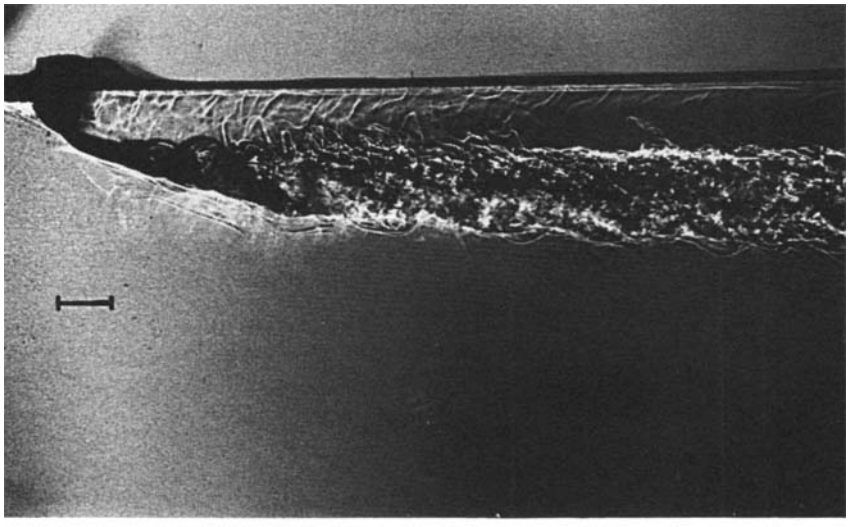

(*c*)

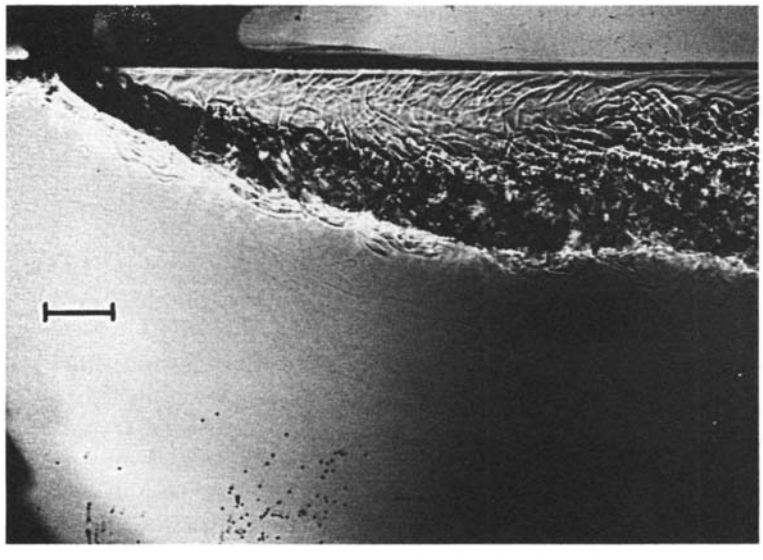

(*d*)

FIGURE 4. Shadowgraphs of stationary density currents produced by various control methods. (*a*) Step displacement device at the bottom of the channel, $U = 4.6$ cm/s, $H = 15.4$ cm, $g' = 3.72$ cm/s^2, $h = 1.05$ cm, $\Delta h = 2.2$ cm; (*b*) barrier device at the bottom, $U = 4.6$ cm/s, $H = 15.4$ cm, $g' = 3.72$ cm/s^2, $h = 2.3$ cm, $\Delta h = 2.2$ cm; (*c*) barrier device at the surface, $U = 5.1$ cm/s, $H = 15.75$ cm, $g' = 3.14$ cm/s^2, $h = 1.2$ cm, $\Delta h = 1.85$ cm; (*d*) suction at the surface, $U = 4.6$ cm/s, $H = 17.5$ cm, $g' = 7.64$ cm/s^2, $h = 3.2$ cm, $\Delta q = 4.3$ cm^2/s. Bar length is 2 cm.

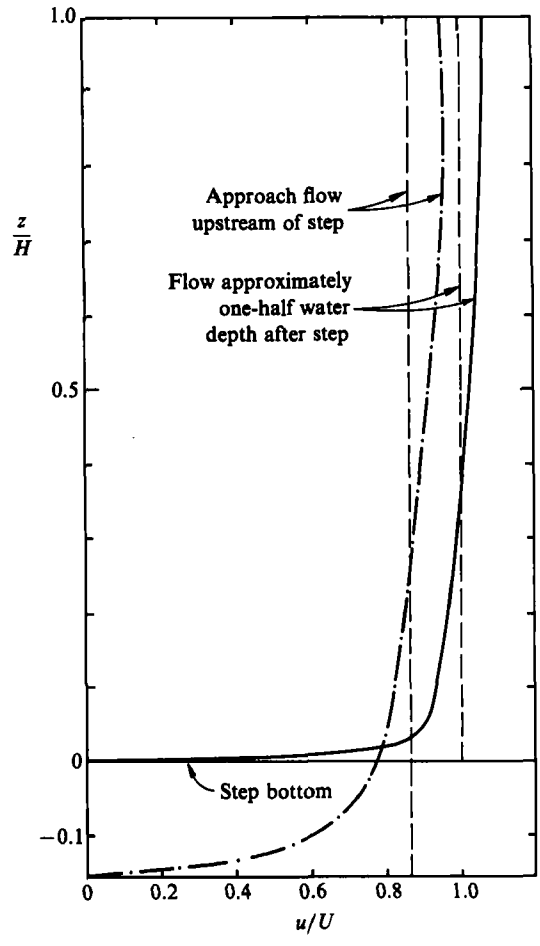

FIGURE 5. Modification of the channel-flow velocity profile due to a step with height equal to the displacement thickness.

The effect of a small barrier (2.2 cm in height) located at the bottom, or of a similar one (1.7 cm in height) located at the surface, are shown in figure 4(*b* and *c*) respectively. The surface-barrier height was chosen from velocity measurements in the underflow under a surface contamination film that formed once an obstruction was put across the flow surface. Under typical experimental conditions the upstream film length grew at a rate of 0.5–1 m per 10 minutes. The flow structure for both barrier cases is qualitatively similar to that for the step displacement device, even though the flow layer corresponding to the barrier height is now occupied by buoyant fluid. (Note that a small amount of buoyant fluid is visible upstream of the barrier. This occurred due to the 'leakage' in the sidewall boundary layers of the flume, but was dynamically insignificant and did not degrade the long-term stability of the flow).

Lastly, figure 4(*d*) displays the effect of a suction device that is placed across the free surface (1 mm immersion, 5 mm slot width). The device withdraws a small amount of flow at a rate corresponding to 5 % of the ambient discharge. The suction removes primarily the ambient-flow layer near the free surface along with any viscous contamination effects. As shown by buoyancy measurements, however, some buoyant

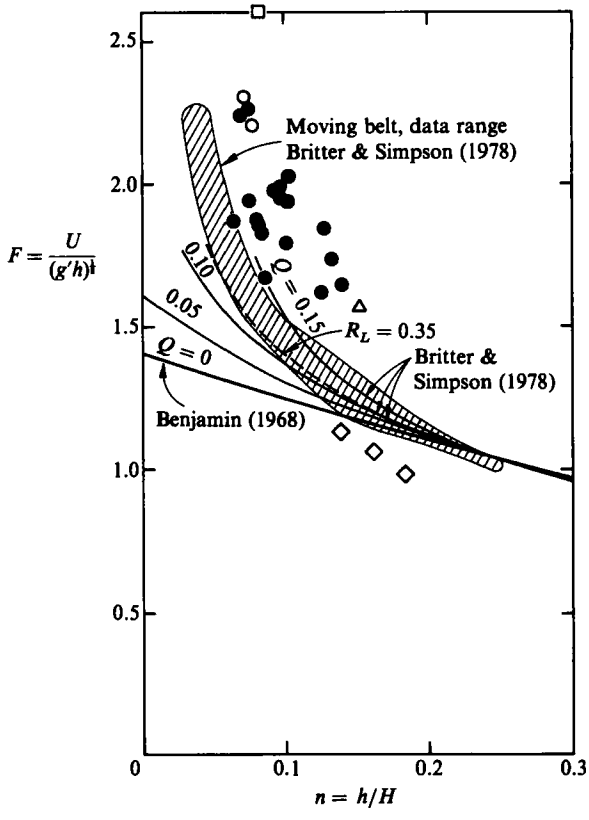

FIGURE 6. Comparison of steady-state density-current data with flow-force theories of Benjamin (1968) and Britter & Simpson (1978) neglecting second-order effects. Data: ●, step device (Sargent & Jirka, 1982); ○, step device; □, barrier device; ◇, suction control.

flow (typically 25–40 % of the total suction flow) is also sucked off in the process. The suction method appears to be the most effective method for maintaining steady density currents that behave like the ideal inviscid model for the current front.

In figure 6 the experimental data are compared with the flow-force theory of Benjamin, (1), with the expanded flow-force theory of Britter & Simpson that includes mixing in the head-wake zone through a dependence on the unspecified parameter $Q = qg'/U^3$ (or alternatively a shear-layer Richardson number $R_L = g'h_w/\Delta U^2$, where ΔU and h_w are the velocity difference and height of the wake zone with $R_L = 0.35$ as a best fit equilibrium value in agreement with Thorpe's (1973) work on billowing and with Britter & Simpson's moving-belt experiments. In these comparisons U is taken as the depth-averaged velocity at the location of either device (step, barrier or suction) and h is the layer thickness relative to the elevation of either device.

Using Benjamin's model as the first-order prediction of density-current dynamics, the data in figure 6 indicate that the boundary-control manipulations induce other second-order effects in addition to head mixing already considered by Britter & Simpson. It is useful to analyse these second-order effects and define the magnitude of an effective mean velocity U_{eff} that controls the density-current force balance. In Appendix A an analysis is given for the ambient flow over the step device (or barrier), which shows that U_{eff} is smaller than the mean velocity U over the device. The flow

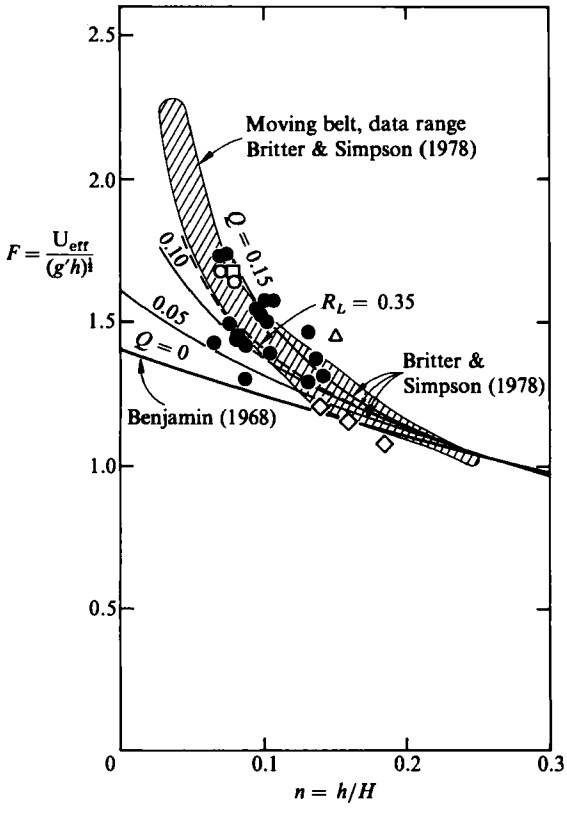

FIGURE 7. Comparison of steady-state density-current data with flow-force theories after accounting for second-order effects produced by the control methods. Symbols as on figure 6.

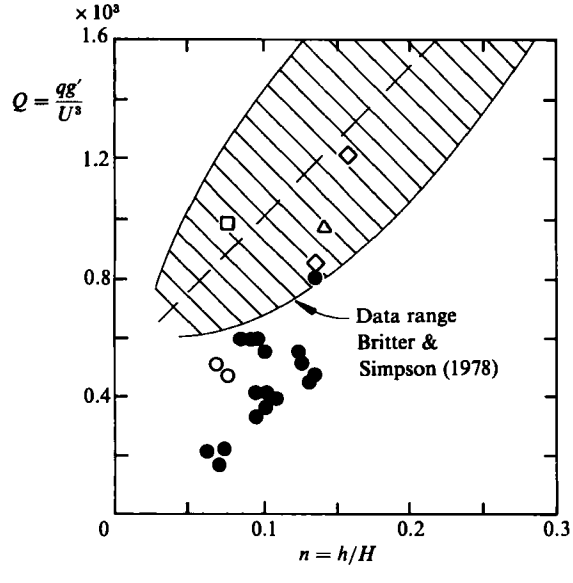

FIGURE 8. Head entrainment rates as a function of layer thickness. Symbols as on figure 6.

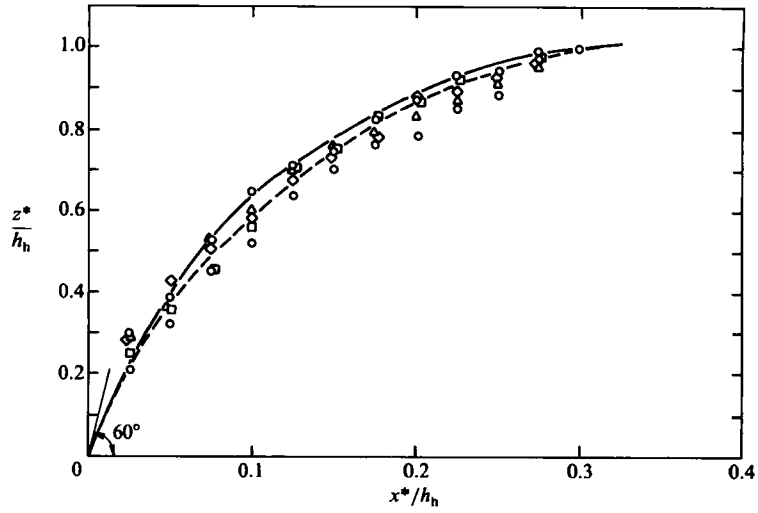

FIGURE 9. Head shape (x^*, z^*) normalized with total head height h_n for different control methods, ——, Britter & Simpson (1978), moving belt; – – – –, Sargent & Jirka (1982), step device; other symbols as on figure 6.

stagnation pressure at the device shoulder is reduced since the flow originates in the upstream boundary layer. On the other hand, the suction-flow analysis in Appendix B gives U_{eff} larger than U as the suction pushes the stagnation point away from the boundary elevation. This increased potential energy causes a larger intrusion pressure to be balanced by the available kinetic energy of the flow. The effective velocity changes are of order $\pm 20\,\%$ for the present experimental conditions and are presented in figure 7 which shows a satisfactory agreement with the data of Britter & Simpson.

A summary of normalized entrainment rates $Q = qg'/U^3$ as a function of layer thickness n is given in figure 8. With the exception of the bulk of the step-displacement experiments, which show somewhat lower rates, the various data are in reasonable agreement with Simpson & Britter's data and indicate increasing entrainment with increasing current thickness. Similarly, the normalized head shape for the different experimental configurations (figure 9) shows little variability. In any case – except possibly the suction device (see also figure 4*d*) – the slope of the foremost point is somewhat less than the theoretical 60° slope. Exact observations are difficult, however, owing to the small scale of the flow and to lateral and temporal variability.

5. Concluding remarks

Starting with a perturbation analysis of an inviscid approach flow, we have shown that the observed bifurcation of a density intrusion into either a density current or a density wedge is governed by momentum changes in the ambient flow relative to the inviscid case. Any momentum deficit – typically due to boundary-layer formation in the ambient flow – results in the eventual formation of a density wedge in a uniform channel geometry. On the other hand, a momentum surplus is needed in a uniform channel to support in a steady-state a stable density current. Furthermore, small non-uniformities installed in the channel – referred to as control methods – also assure stable density currents by controlling the small-scale viscous effects of the ambient flow. In analogy to fluid–solid interaction, the density wedge is governed

by interfacial (skin-friction) drag, while pressure drag dominantes the density-current dynamics.

Several exploratory experiments have shown that a variety of boundary-layer control methods (steps, barriers or suction) can be used to prevent wedge intrusions over long distances in ambient-flow situations in which a boundary layer exists. In all of these methods a small local manipulation – of the order of 10% – of a primary flow variable (e.g. ambient depth or ambient discharge) is employed in order to stabilize a density current at a fixed location. If proper account is taken of the second-order dynamic effects of these manipulations, then the observed density current forms and force balances are all similar to each other and in agreement with the fundamental theory of Benjamin (1968) and its amplification, including head mixing, by Britter & Simpson (1978).

Apart from their experimental convenience for the study of steady-state density currents, the proposed boundary-layer control methods may have a great potential for engineering design and environmental protection. The control methods, notably the small barrier and the suction, or combinations and modifications thereof, would be effective for the prevention of long-distance intrusions into ambient shear flows of undersirable or noxious fluids. Applications may include ventilation of mines, air quality control in buildings, containment of oil pollution or gas spills, prevention of salt water (often also sediment laden) intrusion into coastal rivers or waterways and design of thermal effluent discharges, cooling ponds and solar ponds.

Finally, we want to emphasize that the present analysis and experiments were limited to a two-dimensional framework, with one horizontal (streamwise) direction and the vertical direction aligned with gravity. As mentioned, in a wide channel the effect of the lateral wall boundary layer appears to be negligible. More complex interaction possibilities exist, however, when oblique or curved intrusion fronts are considered with variation in the second horizontal (spanwise) direction. For example, the front produced by a stationary radial buoyant source discharging at the surface of a crossflowing water body was found (Jirka 1980; Jones & Jirka 1986) to be of the density-current type. All surface contamination is swept along the curved front. It does not accumulate locally and, therefore, does not cause the gradual breakdown to a density wedge as in the two-dimensional case.

This research was supported in part by the US National Science Foundation, Grant No. CME-8012682. We would like to thank the referees for several suggestions – including the reference to the recent work of Rottman *et al.* (1985) – that substantially improved the manuscript.

Appendix A. Flow over a displacement step (or barrier)

We first consider the ambient flow over a step device in the absence of a density current (see figure 10). The device height Δh is approximately equal to the displacement thickness in the ambient shear flow. Hence, the velocity profile U at the top of the rounded step is approximately uniform, as validated by the experiments. A global energy equation between a section 1 upstream of the device and a section 2 just at the step yields, neglecting energy losses over this short distance,

$$\rho_1 \alpha_1 \frac{V^2}{2} + \rho_1 g(H + \Delta h + \delta_H) = \rho_1 \alpha_2 \frac{U^2}{2} + \rho_1 g(H + \Delta h), \tag{A 1}$$

in which V is the average velocity upstream, δ_H the change (drop) in surface profile over the device and H the water depth in section 2. α_1 and α_2 are energy correction

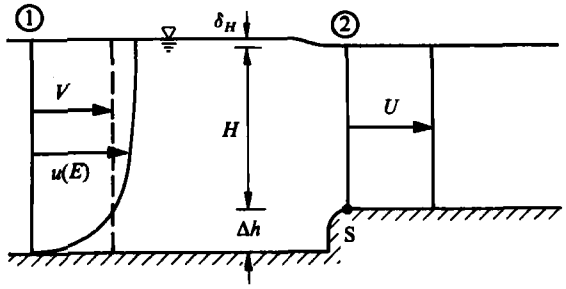

FIGURE 10. Ambient free-surface flow with solid floor boundary layer over step displacement device.

factors; henceforth, α_1 will be taken as 1.045 corresponding to the one-seventh law in the fully established ambient flow and $\alpha_2 \approx 1$, neglecting the thin boundary layer that develops. Hence,

$$\delta_H = \frac{1}{2g}(U^2 - \alpha_1 V^2). \tag{A 2}$$

Furthermore, a local energy equation for a streamline that passes close to the top of S at the shoulder of the device and that originates within the boundary layer of the ambient flow is written

$$\rho_1 \alpha_\Delta \frac{V^2}{2} + \rho_1 g(H + \Delta h + \delta_H) = p_S + \rho_1 g \Delta h, \tag{A 3}$$

in which p_S is the total stagnation pressure at S and α_Δ is the kinetic energy factor for the displaced boundary layer, defined by

$$\alpha_\Delta V^3 \Delta h = \int_0^{\Delta h} u^3 \, dz. \tag{A 4}$$

$u(z)$ is the velocity profile, characterized by the one-seventh law,

$$\frac{u}{u_{\max}} = \left(\frac{z}{H + \Delta h}\right)^{\frac{1}{7}}. \tag{A 5}$$

With $V = \frac{7}{8}u_{\max}$, this yields

$$\alpha_\Delta = \left(\frac{8}{7}\right)^3 \left(\frac{7}{10}\right) \left(\frac{\Delta h}{H + \Delta h}\right)^{\frac{3}{7}} = \alpha_1 \left(\frac{\Delta h}{H + \Delta h}\right)^{\frac{3}{7}}. \tag{A 6}$$

For our typical experimental conditions ($H = 15.4$ cm, $\Delta h = 2.2$ cm) $\alpha_\Delta = 0.44$. The continuity equation, $V = UH/(H + \Delta h)$ to first order, together with (A 2) and (A 3) gives

$$p_S = \rho_1 \frac{U^2}{2} \left\{ \alpha_\Delta \left(\frac{H}{H + \Delta h}\right)^2 + \left[1 - \alpha_1 \left(\frac{H}{H + \Delta h}\right)^2\right] \right\} + \rho_1 g H. \tag{A 7}$$

Once a dense fluid is introduced, it is the stagnation pressure p_S that causes arresting of the current at the step shoulder S. Hence, the mean velocity U, depth H and stagnation pressure p_S are the parameters governing the force balance with the density current (buoyancy g' and thickness h). In the simplest case of zero head entrainment this balance is given by Benjamin's (1968) equations, a momentum equation (with the usual Boussinesq simplifications)

$$U^2 \frac{Hh}{H - h} = -\tfrac{1}{2} g' h^2 + g \delta H, \tag{A 8}$$

and a Bernoulli equation for the hydrostatic conditions in the dense flow

$$p_S = \rho_1 g(H-h-\delta)+\rho_2 gh, \tag{A 9}$$

in which δ is the surface drawdown over the density current. (Note that Britter & Simpson's (1978) model with head entrainment could also have been introduced at this point at the expense of additional complexity.)

Combining (A 7), (A 8) and (A 9) gives

$$\frac{U^2}{g'h} = \frac{(2-n)(1-n)}{2n+(1-n)\left[1+\frac{\alpha_\Delta-\alpha_1}{(1+\Delta)^2}\right]}, \tag{A 10}$$

with $n = h/H$ and $\Delta = \Delta h/H$. Equation (A 10) can now be compared to the classical Benjamin equation (see (1)), written as

$$\frac{U_{\text{eff}}^2}{g'h} = \frac{(2-n)(1-n)}{(1+n)}, \tag{A 11}$$

in which U_{eff} denotes the ideal inviscid nature of the uniform approach flow. Comparing (A 10) and (A 11) gives

$$U_{\text{eff}} = U\left\{\frac{2n}{1+n}+\frac{1-n}{1+n}\left[1+\frac{\alpha_\Delta-\alpha_1}{(1+\Delta)^2}\right]\right\}^{\frac{1}{2}}. \tag{A 12}$$

For the present experiments the square-root factor is of the order of 0.80, less than unity. Thus, the effective velocity that actually arrests the density current is lower than the mean ambient velocity over the device. This is due to the low energy content ($\alpha_\Delta < 1$) of the flow on the upstream boundary layer that gets mixed and squeezed when flowing over the step device.

Identical arguments would pertain to the use of a rounded barrier of height Δh instead of a step device: the conditions at the top of the barrier would be similar to those at section 2 in figure 10. The thickness h of the density current is measured relative to the top of the barrier, however.

Appendix B. Suction flow

We analyse the simplest case of a suction flow, namely one with an inviscid approach flow and neglecting head entrainment (see figure 11). The real fluid effects could readily be introduced into the basic model below by combining it with the analyses of Appendix A and Britter & Simpson.

The bulk momentum equation between sections 1 and 2 is

$$\rho_1 U_2^2(H-h-\delta)-\rho_1 U^2(H-l) = \tfrac{1}{2}\rho_1 gH^2-\tfrac{1}{2}\rho_1 g(H-\delta)^2-\tfrac{1}{2}(\rho_2-\rho_1)gh^2, \tag{B 1}$$

where l is the withdrawal-layer thickness in the ambient flow. In (B 1) the momentum fluxes due the withdrawal flows Δq, and Δq_2 are assumed to be balanced by pressure forces on the suction slot. Continuity equations are

$$UH = U_2(H-h-\delta)+\Delta q_1, \tag{B 2}$$

$$Ul = \Delta q_1, \tag{B 3}$$

$$\Delta q = \Delta q_1+\Delta q_2. \tag{B 4}$$

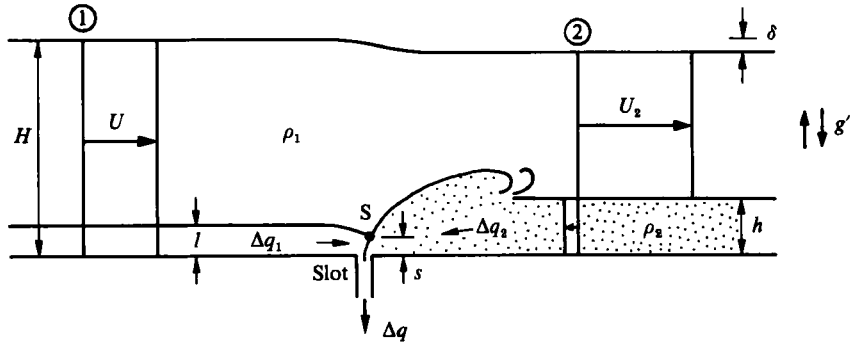

FIGURE 11. Interaction of inviscid ambient flow, density current and suction flow.

Bernoulli equations in each fluid yield the stagnation pressure

$$\rho_1 \frac{U^2}{2} + \rho_1 gH = p_S + \rho_1 gs, \tag{B 5}$$

$$\rho_1 g(H-h-\delta) + \tfrac{1}{2}\rho_2 \left(\frac{\Delta q_2}{h}\right)^2 + \rho_2 gh = p_S + \rho_2 gs. \tag{B 6}$$

A simple estimate for the elevation s of the stagnation point S is obtained as follows. An inner approximation for the localized withdrawal flow through the narrow (line) slot is a radial velocity distribution $v_w = \Delta q/(\pi r)$, where r is the radial distance, which is unaffected by the density field (reference density ρ_0). Hence, the local pressure deviation p_w from the externally imposed stagnation pressure is given by $p_w = \frac{1}{2}\rho_0 v_w^2$, which satisfies $p_w \to 0$ as $v_w \to 0$ outside the zone of withdrawal influence $r \to \infty$. As an outer approximation within the buoyancy field g', that pressure disturbance causes an uplift z above the bottom of the equipotential surfaces $z = -p_w/(\rho_0 g')$. In particular, for the dividing streamline on which S is located at a distance r along the radius $\theta = \pi\Delta q_2/\Delta q$ the uplift is given by $s = v_s^2/2g'$ in which v_s is the inner velocity at distance r_s. Using the geometric relation $s = r_s \sin\theta$, and the above relationships the uplift elevation for the stagnation point becomes

$$s = \left[\frac{1}{2g'}\left(\frac{\Delta q}{\pi}\left(\sin \pi \frac{\Delta q_2}{\Delta q}\right)\right)^2\right]^{\frac{1}{3}}. \tag{B 7}$$

Given U, H, ρ_1, ρ_2, g and Δq, the seven equations above yield the seven unknowns h, U_2, δ, p_S, s, Δq_1 and l, provided that the flow rate Δq_2 is also externally imposed. If the latter provision is not met, then some additional critical relationship is needed that controls the flow distribution into Δq_1 and Δq_2 subject to the total suction flow Δq. Alternatively, we can assume that the dividing streamline is still governed by its first-order balance with an angle $\theta = \frac{1}{3}\pi$ so that the flow is distributed as $\Delta q_1 \approx \frac{2}{3}\Delta q$ and $\Delta q_2 \approx \frac{1}{3}\Delta q$. Indeed, this simplification agrees with our observations on the buoyancy concentration in the suction flow (see §4). The solution of the equation system is then

$$\frac{U^2}{g'h} = \frac{(1-n)\,[2(1-s^*)-n]}{2(1-\frac{2}{3}q^*n)\,(n-\frac{2}{3}q^*n)+(1-n)-\left(\frac{q^*}{3}\right)^2(1-n)}, \tag{B 8}$$

in which $n = h/H$, $q^* = \Delta q/(Uh)$ and

$$s^* = \frac{s}{h} = \left[\frac{3\Delta q^2}{8g'\pi^2 h^3}\right]^{\frac{1}{3}}. \tag{B 9}$$

If this solution is compared to Benjamin's reference solution (with suction) as was done in Appendix A, (A 11), the effective velocity that causes stagnation is related to the mean velocity by

$$U_{\text{eff}} = U\left\{\frac{(2-n)\,2n(1-\frac{2}{3}q^*)\,(1-\frac{2}{3}q^*n)+(1-n)\left(1-\left(\frac{q^*}{3}\right)^2\right)}{(1+n)\,[2(1-s^*)-n]}\right\}^{\frac{1}{2}}. \tag{B 10}$$

For our typical run conditions (B 10) indicates that $U_{\text{eff}}/U \approx 1.10$. Typical predicted stagnation elevations for the experiments are 0.5 cm in agreement with dye flow visualization. Thus, the suction flow affects the dynamic balance through lift-up of the stagnation point, which acts like a barrier effect so that a larger layer depth h can be supported with a given approach velocity U. Qualitatively, this lift-up effect is similar to the elevated-nose effect for a density current advancing over a solid bottom (Simpson & Britter 1979).

REFERENCES

Batchelor, G. K. 1967 *An Introduction to Fluid Dynamics*. Cambridge University Press.

Benjamin, T. B. 1968 Gravity currents and related phenomena. *J. Fluid Mech.* **31**, 209–248.

Britter, R. E. & Simpson, J. E. 1978 Experiments on the dynamics of a gravity current head. *J. Fluid Mech.* **88**, 223–240.

Jirka, G. H. 1980 Two-dimensional density current form continuous source in stratified crossflow. In *Proc. 2nd Intl Symp. on Stratified Flows* (ed. T. Carstens). Trondheim, Norway.

Jones, J. M. & Jirka, G. H. 1986 Transcritical stratified flow from a buoyant source in a cross-current. *J. Geophys. Res.* (submitted).

Kármán, Th. von 1940 The engineer grapples with non-linear problems. *Bull. Am. Math. Soc.* **46**, 615–683.

Rottman, J. W., Hunt, J. C. R. & Mercer A. 1985 The initial and gravity-spreading phases of heavy gas dispersion: comparison of models with phase I data. *J. Hazardous Materials* **11**, 261–279.

Sargent, F. E. & Jirka, G. H. 1982 A comparative study of density currents and density wedges. *Tech. Rep.* School of Civil and Environmental Engineering, Cornell University, Ithaca, New York.

Schijf, J. B. & Schonfeld, J. C. 1953 Theoretical considerations on the motion of salt and fresh water. *Proc. Minnesota Intl Hydraul. Conv.* p. 321. ASCE and IAHR.

Simpson, J. E. 1982 Gravity currents in the laboratory, atmosphere, and ocean. *Ann. Rev. Fluid Mech.* **14**, 213–234.

Simpson, J. E. & Britter, R. E. 1979 The dynamics of the head of a gravity current advancing over a horizontal surface. *J. Fluid Mech.* **94**, 477–495.

Simpson, J. E. & Britter, R. E. 1980 A laboratory model of an atmospheric mesofront. *Q. J. R. Met. Soc.* **106**, 485–500.

Thorpe, S. A. 1973 Turbulence in stably stratified fluids: A review of laboratory experiments. *Boundary-Layer Met.* **5**, 95–119.

Turner, J. S. 1973 *Buoyancy Effects in Fluids*. Cambridge University Press.